

# DESIGNING AN ARTIFICIAL INTELLIGENCE-BASED MODEL FOR ELECTRIC MOTOR FAULT DIAGNOSIS TO SUPPORT MAINTENANCE DECISION-MAKING

Ho-Si-Hung Nguyen<sup>1</sup>, Thi-Hoang-Giang Tran<sup>1\*</sup>, Manh-Tien Luu<sup>1</sup>, Huy-Vu Tran<sup>2</sup>

<sup>1</sup>The University of Danang - University of Science and Technology, Vietnam

<sup>2</sup>Central Power Electronic Measurement Equipment Manufacturing Center, Vietnam

\*Corresponding author: tthgiang@dut.udn.vn

(Received: April 22, 2024; Revised: May 21, 2024; Accepted: May 27, 2024)

**Abstract** - Motors play a crucial role in production systems. However, not everything always goes smoothly, and motor failures are one of the common challenges in the production process. Misalignment of the drive shaft is a frequent motor fault caused by improper installation or damage to machine components. This study proposes the design of a monitoring and fault diagnosis model for DC motors, which includes: (i) a PID controller for motor speed control; (ii) a vibration signal acquisition unit; and (iii) a motor monitoring unit via Blynk and signal processing for fault diagnosis. In the model, motor faults are classified using a convolutional neural network (CNN) based on analog signals that have been transformed to the frequency domain and denoised. Experimental results demonstrate that classification using the convolutional neural network is highly accurate and stable.

**Key words** - Drive shaft misalignment; PID controller; motor monitoring; convolutional neural network.

## 1. Introduction

Electric motors are crucial components in industrial production systems. Most motors are normally recorded to operate reliably and stably. However, there's a possibility that they encounter unforeseen failures when working in harsh environments. Common motor failures include winding faults, rotor and stator imbalance, broken rotors, air gap eccentricity, and bearing faults [1-4]. These faults reduce the motor's operational efficiency, leading to increased energy consumption and potential breakdowns. In practice, early diagnosis of motor faults is essential to make appropriate maintenance decisions, in order to minimize potential damage. To achieve this, the operating condition of motors needs to be monitored regularly or even continuously to ensure stable and safe operation. Various sensor measurements are utilized for online monitoring of motor conditions, and the collected data is subsequently analyzed to identify potential motor faults [3].

Common measurement signals for diagnosing motor faults include stator voltage and current [5-6], air gap eccentricity and external flux density [7], rotor position and speed [8], temperature [9], sound [10], and vibration [11].

Analyzing motor vibration signals to detect faults and assess motor health is a method that has been adopted by many researchers. Vibration signal analysis is highly effective in identifying mechanical faults. Vibrations caused by asymmetries can result from the following mechanical faults: mechanical imbalance, bearing failures, shaft misalignment, and air gap deformation. Additionally, vibrations are also produced due to the imbalance of the magnetic field caused

by electrical factors in the stator windings, such as voltage imbalances and short circuits. Since motor vibrations originate from mechanical, magnetic, and aerodynamic sources, motor fault diagnosis based on motor vibrations is highly appropriate. Vibration-based condition monitoring allows for the detection of 90% of faults or failures in machinery, as each component of the system/equipment has distinct vibration signatures that are closely related to the operating conditions of the machinery [12].

With the rapid development and adoption of IoT in smart factories, the amount of data collected is increasing rapidly. Additionally, the recent groundbreaking advancements in artificial intelligence techniques contribute to the promotion of knowledge-based motor fault diagnosis methods. Knowledge-based approaches, also known as data-driven approaches, utilize large volumes of historical data to extract motor characteristics. Unlike model-based approaches, data-driven approaches do not require extensive information about the machine structure, thus enabling analysis without requiring significant expert knowledge [13]. Data-driven methods often employ statistical and probabilistic analysis, as well as artificial intelligence techniques, including machine learning and deep learning.

In line with these trends, this study focuses on the detection and classification of motor faults based on artificial intelligence, with an emphasis on detecting shaft misalignment. Causes of misalignment may include improper installation, erosion and damage to components due to machine vibrations. Misalignment can lead to bearing failures, bent or worn-out housing, and worn crankshafts and couplings. Therefore, maintaining precise connection is crucial to ensure safe and reliable operation. Specifically, this research develops an experimental model for motor fault diagnosis. The core of this study proposes a method for detecting motor shaft misalignment by analyzing motor vibration signals using a deep learning approach. Experimental results demonstrate that the differences in vibration signals can effectively distinguish between normal operating motors and those experiencing faults.

## 2. Design of the motor fault diagnosis model

### 2.1. Experimental motor model

Figure 1 illustrates the experimental motor model used in this study. The model consists of: (A) a DC motor, (B) a rotating shaft, (C) two bearings, (D) a weight disk mounted

on the shaft, (E) a coupling, (F) proximity sensors measuring positional deviations to capture vibration signals, and (H) a control and signal acquisition unit. The collected signals are sent to a computer via Wifi using the TCP/IP protocol.

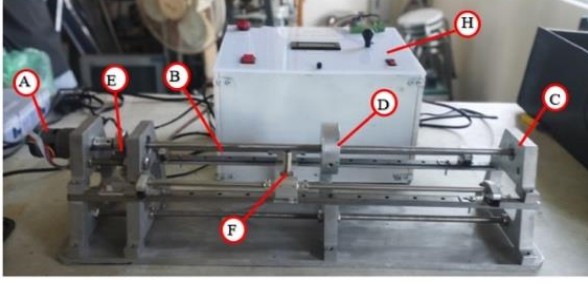


**Figure 1.** Experimental model

(A) Motor; (B) Shaft; (C) Bearing; (D) Weight disk; (E) Coupling; (F) Proximity sensors; (H) Control unit

To create a dynamic imbalance, a weight disk (D) is mounted on the shaft (B) between the two bearings (C). This weight disk has a diameter of 75 mm and a thickness of 25 mm.

## 2.2. Methods and process for implementing the motor fault diagnosis model

To simulate shaft misalignment faults at different speeds while monitoring the operational state, the system is constructed as shown in the diagram in Figure 2. It comprises three components: (i) a PID controller for motor speed control; (ii) a vibration signal acquisition unit; and (iii) a motor monitoring unit via Blynk, including DC motor fault signal processing.

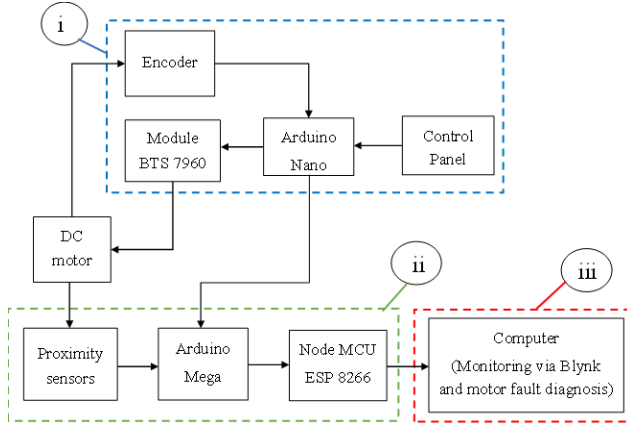


**Figure 2.** Block diagram of the fault diagnosis system

### 2.2.1. PID controller

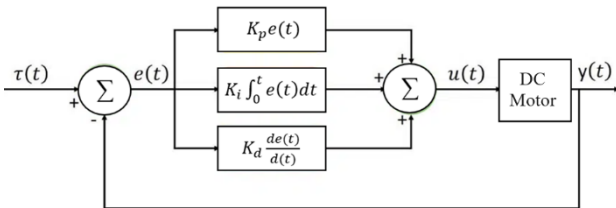


**Figure 3.** Block diagram of PID speed control system

The DC motor speed control model is presented in Figure 3. Here,  $\tau(t)$  is the desired speed,  $u(t)$  is the output signal of the PID controller  $y(t)$  is the motor output signal

(actual motor speed obtained from the encoder), and  $e(t)$  is the difference between the desired speed and the actual speed. The  $e(t)$  signal is transmitted to the PID control unit to stabilize the motor speed.

The PID controller (Proportional-Integral-Derivative) is a common feedback control algorithm used for DC motor speed control. The PID controls the output signal based on the comparison between the measured (actual) value and the target (desired) value. The signal equation  $u(t)$  is as follows:

$$u(t) = K_p \cdot e(t) + K_i \cdot \int_0^t e(\tau) \cdot d\tau + K_d \cdot \frac{de(t)}{dt} \quad (1)$$

Where:  $K_p$  is the proportional gain,  $K_i$  is the integral gain, and  $K_d$  is the derivative gain.

From equation (1), the transfer function can be inferred as follows:

$$G(s) = \frac{u(t)}{e(t)} = K_p + \frac{K_i}{s} + K_d \cdot s \quad (2)$$

To implement the PID control unit, we combine an Arduino Nano microcontroller with a BTS7960 motor driver module. The Arduino Nano serves as the central unit of the control system. After receiving the motor speed signal from the encoder, the Arduino Nano uses the programmed PID controller to process and adjust the motor speed. The PID control output is then fed into the BTS7960 driver to control the motor speed. The connection diagram is shown in Figure 4.

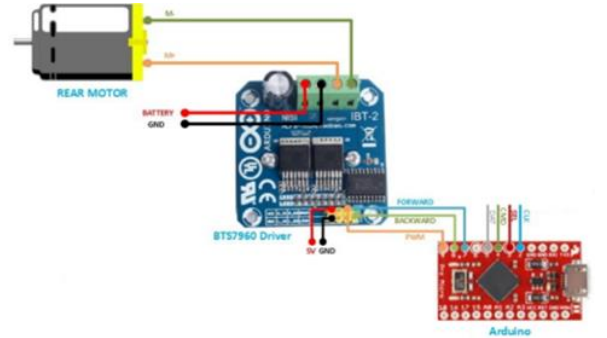


**Figure 4.** Motor control circuit

### 2.2.2. Vibration signal collection kit

Proximity sensors used to collect vibration signals are placed 20 cm away from the bearings. In the normal operating state, no weights are placed on the weight disk. However, to facilitate shaft misalignment during the experiment, a heavy object will be placed at positions 1 through 8 as shown in Figure 5.

Position 1 is parallel to the sensor, with a relative angular deviation of  $0^\circ$  between position 1 and the sensor. The subsequent positions are spaced  $45^\circ$  apart. The weight of the object will be varied in each specific experiment:

*Experiment 1:* No additional weight is placed on the weight disk, corresponding to the normal operating condition of the motor.

*Experiment 2:* A heavy object with a weight of  $m=14$  g is placed on the weight disk and moved to positions 1 through 8.

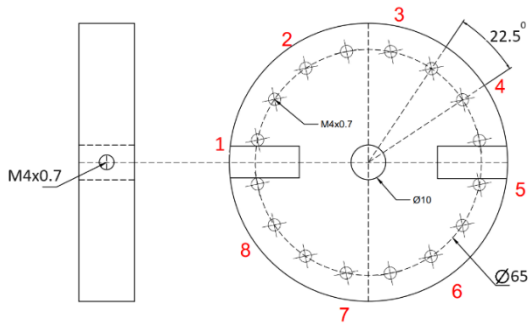


**Figure 5.** Positions of the heavy object on the weight disk

The data from the proximity sensors (measuring positional deviations to capture vibration signals) will be sent to the Arduino Mega microcontroller. The Arduino Mega receives analog voltage signals (0-5V) from the proximity sensors, and communication between the Arduino Mega and Arduino Nano is facilitated via the ESP8266 module using UART communication. The data collecting circuit is shown in Figure 6.

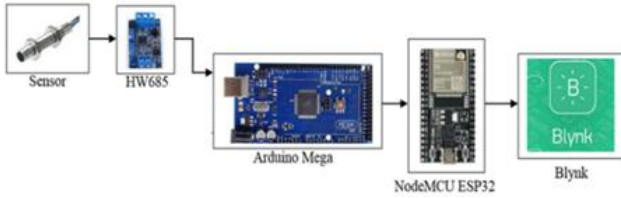


**Figure 6.** Vibration signal collecting circuit

### 2.2.3. Motor monitoring via Blynk and proposed signal processing method for DC motor fault diagnosis

The ESP8266 module enables Wifi connection and communication through the TCP/IP protocol, allowing for data transmission and reception over the Internet. The signals collected from the system are sent to a server for motor control and monitoring. All data is continuously transmitted to Blynk via Wi-Fi. This data is then sent to a computer for DC motor fault diagnosis processing.

To diagnose DC motor faults in this study, the analog signals collected from the sensors are converted to the frequency domain using the Fast Fourier Transform (FFT). The data is then denoised using the Fourier K-means denoising method based on the paper [14].

The denoising process involves four main steps. First, each input data sample is forwardly reversed by FFT. The transformed signal is now a set of real numbers. Next, the frequency spectrum is easily calculated from the previous set of real numbers. Following this, from the obtained frequency spectrum, noise and original signal need to be distinguished based on their amplitudes. A threshold is chosen to separate two types of amplitudes representing featured signals and noise. In this paper, K-means clustering is chosen to act as this threshold to separate the frequency spectrum into two classes ( $K = 2$ ). One class represents noise signals, and the other represents the original signals. In the final step, the featured signals (original signals) in the frequency domain are separated from the noise signals through clustering. Once the original signals are converted to the frequency type and denoised, the signals are further transformed from 1D arrays to 2D arrays (images).

In the final step, a convolutional neural network (CNN) with multiple layers is proposed to perform the task of image classification to recognize and classify shaft misalignment faults. The proposed CNN model is shown in Figure 7.

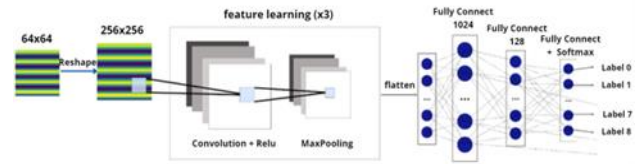


**Figure 7.** Proposed CNN Model

The CNN model includes convolutional layers, pooling layers, and fully connected layers. In this CNN architecture, we use three convolutional layers.

The convolutional layer is a crucial component in the CNN model, as it helps to learn local features from the input images. Each convolutional layer applies a set of filters to perform convolution operations on the input image. The result of the convolution operation is a feature map, where local features are encoded.

In this CNN model, we use three convolutional layers with the following parameters:

- Convolutional Layer 1: 16 filters, filter size 3x3, using ReLU activation function.
- Convolutional Layer 2: 32 filters, filter size 3x3, using ReLU activation function.
- Convolutional Layer 3: 16 filters, filter size 3x3, using ReLU activation function.

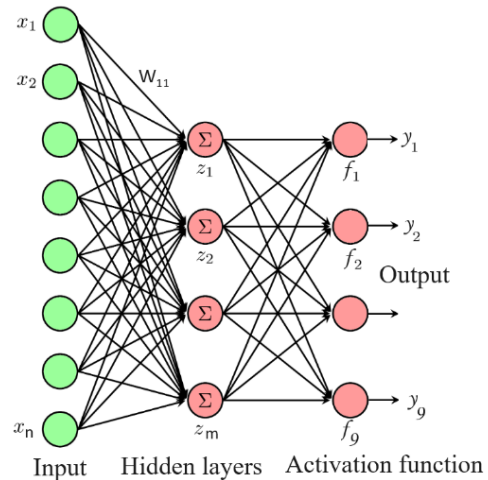


**Figure 8.** Multi-layer Feedforward Neural Network

Behind the convolutional layers, the data is passed to the direct transfer neural network model as shown in Figure 8. In this model, the densely connected layers are fully connected with each other. For the input signal  $x_i$  and the weights connected to the nodes  $w_{ij}$  ( $1 \leq i \leq n$ ;  $1 \leq j \leq m$ ), the value  $z_j$  is:

$$z_j = \sum_{i=1}^n w_{ji} x_i \quad (3)$$

The output function of the  $j^{\text{th}}$  neuron is given by:

$$y_j = f(z_j) \quad (4)$$

Where  $f(z_i)$  is the ReLU activation function for the hidden layers, and  $f(z_j)$  is the softmax activation function for the output layer of the neural network. The ReLU function is used to introduce non-linearity to the layers, while the softmax function provides a probabilistic classification for the output layer.

### 3. Results and evaluation

#### 3.1. PID controller results

The PID parameters were determined experimentally using the Nicole Ziegler method, resulting in  $K_p = 0.003$ ;  $K_i = 0.01$ ;  $K_d = 0.001$ . The experimental results are shown in Figure 9. Figure 9 illustrates the test results with speed increasing from 800 RPM to 1000 RPM. When adjusting the speed, the oscillation process is minimal, and the oscillation time is less than 0.5 seconds before the system reaches and maintains a stable state.

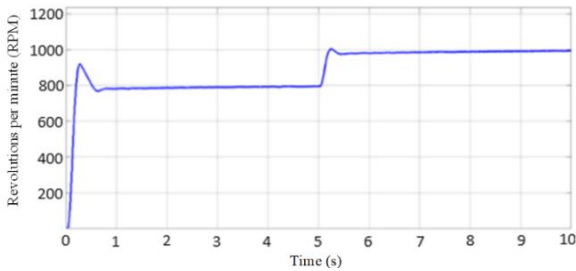


Figure 9. Experimental results of speed increasing from 800 RPM to 1000 RPM

#### 3.2. Results from data collecting kit

The condition without an additional weight on the weight disk can be considered the normal operating state of the motor. The signal collected when the motor is running at a speed of 1000 RPM is shown in Figure 10.

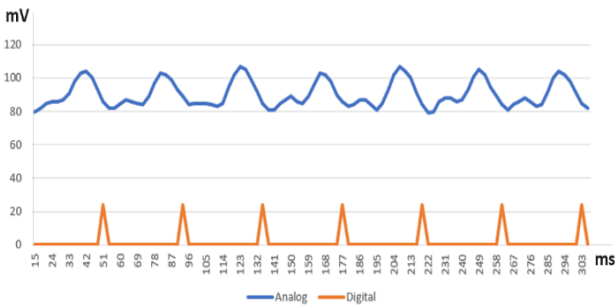


Figure 10. Vibration plot of the motor shaft without additional weight on the weight disk

Clearly, even when the motor operates under normal conditions, there is a slight imbalance vibration on the motor shaft. There are several reasons for this imbalance, such as uneven motor shaft design or unstable motor bearings during rotation, leading to increased imbalance vibrations.

In the case where a weight of  $m = 14\text{ g}$  is placed on the weight disk at positions 1 through 8, the signal collected when the motor is running at a speed of 1000 RPM is shown in Figure 11. It is evident that adding weight significantly increases the vibration amplitude, and the vibration frequency is higher compared to the normal state.

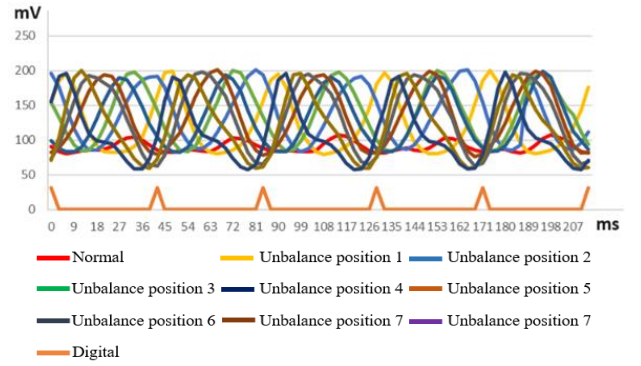


Figure 11. Vibration Plot of the motor shaft when a heavy object with a weight of  $m=14\text{g}$  is placed on the weight disk at positions 1 to 8

#### 3.3. Motor monitoring via Blynk and signal processing for fault diagnosis

##### 3.3.1. Motor monitoring via Blynk

The signals collected from the system are sent to the server to facilitate motor control and monitoring. All data is continuously transmitted to Blynk via Wifi. The application interface is designed to be user-friendly, allowing easy monitoring and control. On the Blynk monitoring interface, one can see the values of motor vibration parameters and motor speed, as shown in Figure 12.



Figure 12. Data displayed on the Blynk Application

##### 3.3.2. Signal processing for fault diagnosis

The data, after being denoised, is categorized into the following cases: no heavy object on the weight disk, and a heavy object placed at each deviation point (8 deviation points) with a mass of  $m=14\text{ g}$ . At each deviation point, measurements were taken using specialized equipment, resulting in 100,000 analog signals (with vibration amplitudes ranging from 50 to 210 mV) with a sampling period of 3 ms per signal. After the denoising step, the signals were converted into plots for each fault and non-fault condition of the motor. These plots were then segmented into sections with a duration of 192 ms. Finally, from the segmented plot frames, we converted them into 2D images as shown in Figure 13. The result is a dataset consisting of 24,000 images of faulty points (3,000 images for each fault point, with 1,000 fault images corresponding to each weight mass) and 600 images of non-fault points, totaling 24,600 images.

In this proposed model, the dataset is divided into three

parts to facilitate the training and validation process. The data ratio for training is 70%, validation is 20%, and testing is 10%.

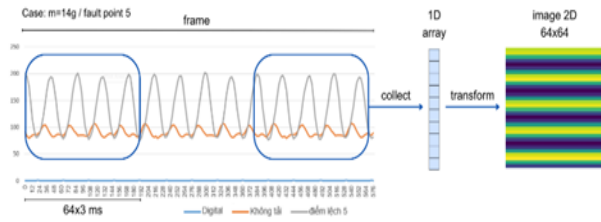


Figure 13. Process of converting analog signal to 2D Image

The process of converting vibration signals into 2D images was applied to all samples in the dataset. Figure 14 displays the images constructed for each fault type at different positions of the heavy object. The labels are numbered from 0 to 8, corresponding to the labels in Table 1.

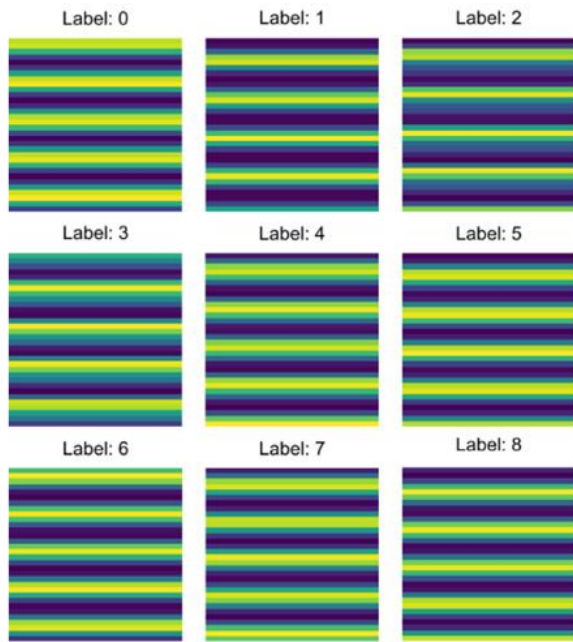


Figure 14. 2D images for different types of faults

Table 1. Explanation of the labels used in the model

Label	Description
0	Fault at deviation point 1
1	Fault at deviation point 2
2	Fault at deviation point 3
3	Fault at deviation point 4
4	Fault at deviation point 5
5	Fault at deviation point 6
6	Fault at deviation point 7
7	Fault at deviation point 8
8	No fault

After training and evaluating the model on the training and validation datasets with 20 epochs, the results in terms of the model's loss and accuracy are illustrated Figure 15. The final results are as follows:

- Loss value on the training dataset: 0.12;

- Loss value on the validation data set: 0.27;
- Accuracy on the training dataset: 0.95;
- Accuracy on the validation dataset: 0.92.

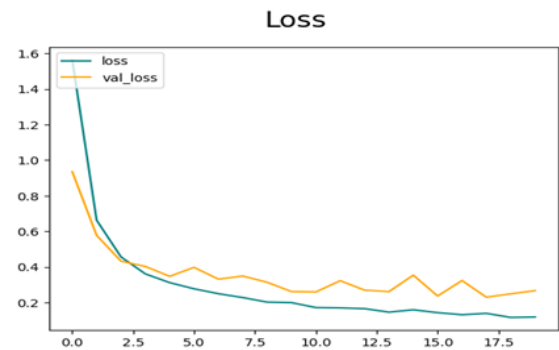
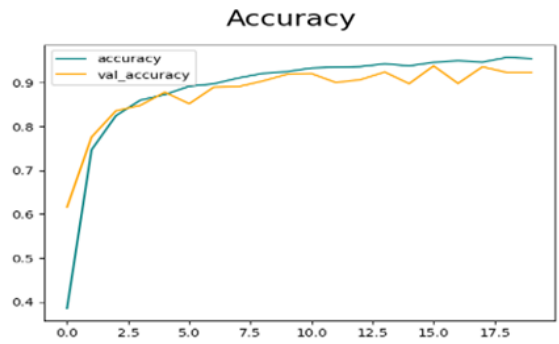


Figure 15. Graph of model accuracy on training and validation datasets and loss value

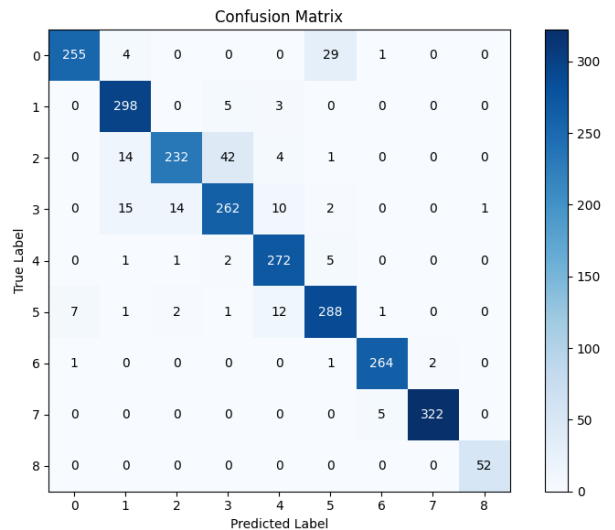


Figure 16. Confusion matrix on the test set

To test the model's accuracy, we performed classification on the test data set. The confusion matrix results are shown in Figure 16, with the following metrics:

- Accuracy (Overall accuracy): 92%
- Precision (Accuracy for positive classes): 98%
- Recall (Coverage for predictions of positive classes): 98%
- F1-score (Harmonic mean between precision and recall): 99%.

The confusion matrix, shown in Figure 16, illustrates the number of predicted labels by the model compared to

the true labels. We observe that the model achieves a good classification accuracy rate of 92% on the test dataset. The most frequent misclassification occurs when the model predicts label 3 as label 2, with 42 instances of such errors; conversely, label 2 is misclassified as label 3 in 14 instances.

From these results, we can see that the trained model accuracy exceeds 90%. Although the model's accuracy is affected by the motor's speed, the model can still learn the features quite well if the training dataset is sufficiently large. The denoising and normalization of data during the preprocessing stage play a crucial role in model training, potentially increasing accuracy by up to 20% compared to unprocessed measurement data.

#### 4. Conclusions

This study has presented the steps for developing a speed monitoring and fault diagnosis model for DC motors. The focus of the research is diagnosing shaft misalignment faults in DC motors. This diagnostic process is based on relatively modern AI technology. The model collects vibration data in the form of analog signals under two conditions: (i) without adding any heavy object to the weight disk, corresponding to normal motor operation, and (ii) with a heavy object of  $m = 14$  g placed at different positions on the weight disk. This data is then transformed into frequency domain plots for each faulty and non-faulty condition of the motor. These plots are segmented into sections with an equivalent range of 192 ms. Subsequently, from the segmented plot frames, they are converted into 2D images. All data is then trained using a convolutional neural network model. The imbalances corresponding to different positions are labeled to identify motor faults for positions 1 through 8. Experimental results show that the CNN-based classifiers achieve high accuracy.

The study is limited by the uneven design of the motor shaft and the instability of motor bearings, which lead to increased imbalance vibrations when the motor operates at high speeds.

**Acknowledgment:** This work was supported by The University of Danang - University of Science and Technology, code number of Project: T2023-02-41.

#### REFERENCES

- [1] M. E. H. Benbouzid, "A review of induction motors signature analysis as a medium for faults detection", *IEEE Transactions on Industrial Electronics*, vol. 47, no. 5, pp. 984–993, 2000.
- [2] A. Siddique, G. S. Yadava, and B. Singh, "A review of stator fault monitoring techniques of induction motors", *IEEE Transactions on Energy Conversion*, vol. 20, no. 1, pp. 106–114, March 2005, doi: 10.1109/TEC.2004.837304.
- [3] P. Tavner, L. Ran, J. Penman, and H. Sedding, *Condition monitoring of rotating electrical machines*, 2nd edition. The Institution of Engineering and Technology, 2008.
- [4] O. V. Thorsen and M. Dalva, "A survey of faults on induction motors in offshore oil industry, petrochemical industry, gas terminals, and oil refineries", *IEEE Transactions on Industry Applications*, vol. 31, no. 5, pp. 1186–1196, 1995.
- [5] K. Laadjal, H. R. P. Antunes, M. Sahraoui, F. Bento, and A. J. M. Cardoso, "Online Diagnosis and Discrimination of Stator Faults in Six-Phase Induction Motors Based on Voltage Symmetrical Components", *IEEE Transactions on Transportation Electrification*, vol. 9, no. 2, pp. 3115–3126, June 2023, doi: 10.1109/TTE.2022.3219722
- [6] P. Przemyslaw and M. Wolkiewicz, "Demagnetization Fault Diagnosis of Permanent Magnet Synchronous Motors Based on Stator Current Signal Processing and Machine Learning Algorithms", *Sensors*, vol. 23, no. 4, pp. 1757, 2023.
- [7] F. Thollon, G. Grellet, and A. Jammal, "Asynchronous motor cage fault detection through electromagnetic torque measurement", *European Transactions on Electrical Power*, vol. 3, no. 5, pp. 375–378, 1993.
- [8] J. Piotrowski, *Shaft alignment handbook*. Crc Press, 2006.
- [9] A. Glowacz, "Thermographic fault diagnosis of ventilation in BLDC motors", *Sensors*, vol. 21, no. 2021, pp. 7245, 2021.
- [10] P. A. Delgado-Arredondo *et al.*, "Methodology for fault detection in induction motors via sound and vibration signals", *Mechanical Systems and Signal Processing*, vol. 83, no. 2017, pp. 568–589, 2017.
- [11] W. Qian and S. Li, "A novel class imbalance-robust network for bearing fault diagnosis utilizing raw vibration signals", *Measurement*, vol. 156, 2020.
- [12] M. Chandrabhanu and I. Panigrahi, "Review of condition monitoring of rolling element bearing using vibration analysis and other techniques", *Journal of Vibration Engineering & Technologies*, vol. 7, pp. 407–414, 2019.
- [13] Z. Gao, C. Cecati, and S. X. Ding, "A Survey of Fault Diagnosis and Fault-Tolerant Techniques-Part I: Fault Diagnosis with Model-Based and Signal-Based Approaches", *IEEE Transactions on Industrial Electronics*, vol. 62, no. 6, pp. 3757–3767, June 2015, doi: 10.1109/TIE.2015.2417501.
- [14] T. D. Khoa, N. H. S. Hung, V. H. Canh, N. Boudaoud, V. T. Dung, and D. D. Hanh, "A New Denoising Method for Motor Fault Diagnosis", *Advances in Integrated Design and Production II, Lecture Notes in Mechanical Engineering*, Springer, Cham, 2023, [https://doi.org/10.1007/978-3-031-23615-0\\_54](https://doi.org/10.1007/978-3-031-23615-0_54).